In-situ synthesis of silicon flake/nitrogen-doped graphene-like carbon composite from organoclay for high-performance lithium-ion battery anode

Article *in* Chemical Communications · February 2019

DOI: 10.1039/C8CC10036E

CITATIONS
3

READS
107

9 authors, including:

Qingze Chen
Chinese Academy of Sciences
22 PUBLICATIONS **353** CITATIONS
SEE PROFILE

Runliang Zhu
Guangzhou Institute of Geochemistry, CAS
177 PUBLICATIONS **2,834** CITATIONS
SEE PROFILE

Qiuzhi He
Chinese Academy of Sciences
6 PUBLICATIONS **11** CITATIONS
SEE PROFILE

Shaohong Liu
Sun Yat-Sen University
43 PUBLICATIONS **1,873** CITATIONS
SEE PROFILE

ChemComm

Accepted Manuscript

ROYAL SOCIETY OF CHEMISTRY

rsc.li/chemcomm

ROYAL SOCIETY OF CHEMISTRY View Article Online
DOI: 10.1039/C8CC10036E

Journal Name

COMMUNICATION

In-situ synthesis of silicon flake/nitrogen-doped graphene-like carbon composite from organoclay for high-performance lithium-ion battery anode

Received 00th January 20xx,
Accepted 00th January 20xx

DOI: 10.1039/x0xx00000x

www.rsc.org/

Qingze Chen[a, b], Runliang Zhu*[a], Qiuzhi He[a, b], Shaohong Liu[c], Dingcai Wu*[c], Haoyang Fu[a, b], Jing Du[a, b], Jianxi Zhu[a], Hongping He[a, b]

Silicon flake/nitrogen-doped graphene-like carbon composite was prepared from organoclay *via* an *in-situ* strategy, involving carbonization followed by low-temperature aluminothermic reduction. The pre-formed carbon sheets within the confined interlayer space of clay acted as nanotemplates for *in situ* synthesizing silicon flakes. As lithium-ion battery anode, the composite exhibited excellent electrochemical properties.

Lithium-ion batteries (LIBs) with high energy/power density have become fundamental energy storage devices in electric vehicles, small electronics, and smart grids.[1, 2] The rising demand for higher energy density has stimulated a surge in improving the performance of LIBs.[3, 4] Silicon (Si) is a promising anode candidate in next-generation LIBs due to its high specific capacity (4200 mAh g^{-1} in a $Li_{22}Si_4$ form), 10 times higher than that of traditional graphite anode.[5, 6] Unfortunately, the practical application of Si anodes in LIBs is hindered by severe capacity decay upon cycling owing to the structural cracking and interfacial instability (resulting from the huge volume change during lithiation/delithiation process).[7] Many efforts have been devoted to dealing with these issues, such as nanostructuring[7, 8] and surface engineering[9, 10]. Among them, combining nanostructured Si with carbon nanomaterial is an effective method to improve the cycling stability of Si anodes.[3] In the Si/C composites, Si nanostructures with high surface-to-volume ratio can effectively withstand the diffusion-induced stress and alleviate the pulverization of Si; carbon nanomaterials not only strengthen the transport property, but also serve as buffer media for mechanical strains.[11, 12]

Graphene is an attractive carbonaceous coating for nanostructured Si owing to its excellent electronic conductivity and mechanical flexibility,[13] and the Si/graphene composites exhibited improved electrochemical performance compared with pure Si.[5] However, several significant difficulties remain for the Si/graphene anodes: 1) Si nanoparticles easily lose electrical contact with graphene sheets due to the repeated volume changes upon cycling, leading to a capacity fading; 2) a good performance requires a highly dispersion of nanostructured Si in graphene matrix, which is hard to achieve by simply mechanical mixing; 3) the synthesis of both nanostructured Si (e.g., *via* electroless/electrochemical etching and chemical vapor deposition (CVD))[14] and graphene (e.g., *via* CVD, mechanical peeling, and chemical/thermal reduction)[15] always depends greatly on high cost and complicated procedures. On the other hand, both theoretical and experimental studies indicated that heteroatoms (e.g., nitrogen or sulfur) doping into graphene can increase electronic conductivity and active sites toward lithium.[16] However, the heteroatom-doping strategies usually consist of the preparation of graphene followed by the introduction of heteroatom,[17] which further make the synthesis of Si/graphene composites rather complex.

Herein, we present a novel and facile strategy for the *in-situ* synthesis of silicon flake/nitrogen-doped graphene-like carbon composite (Si/NG) from organoclay *via* carbonization

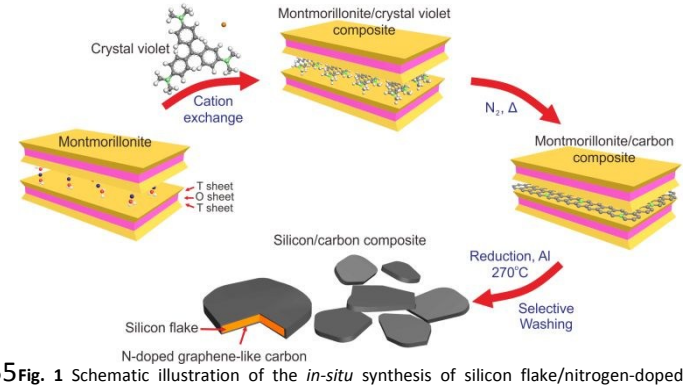

Fig. 1 Schematic illustration of the *in-situ* synthesis of silicon flake/nitrogen-doped graphene-like carbon composite from montmorillonite/crystal violet composite.

[a] *CAS Key Laboratory of Mineralogy and Metallogeny, Guangdong Provincial Key Laboratory of Mineral Physics and Materials, Guangzhou Institute of Geochemistry, Chinese Academy of Sciences, Guangzhou 510640, China. E-mail: zhurl@gig.ac.cn*
[b] *University of Chinese Academy of Sciences, Beijing 100049, China.*
[c] *Materials Science Institute, PCFM Lab and GDHPRC Lab, School of Chemistry, Sun Yat-sen University, Guangzhou 510275, China. E-mail: wudc@mail.sysu.edu.cn*

† Electronic Supplementary Information (ESI) available: Experimental details; auxiliary analysis. See DOI: 10.1039/x0xx00000x

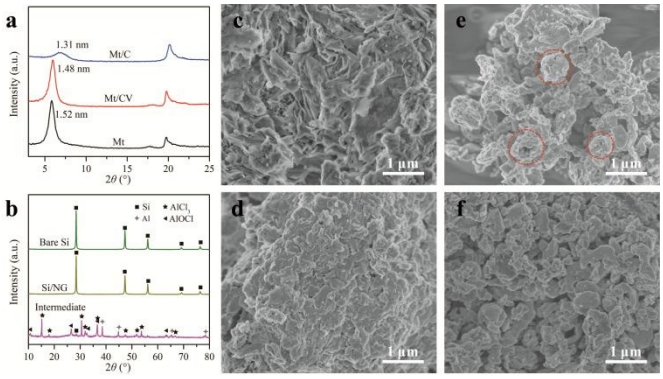

Fig. 2 (a) XRD patterns of Mt, Mt/CV, and Mt/C. (b) XRD patterns of the intermediate after reduction reaction using Mt/C as precursor, the corresponding product Si/NG, and the product bare Si using Mt as precursor. SEM images of the pristine Mt (c), Mt/C (d), bare Si (e), and Si/NG (f).

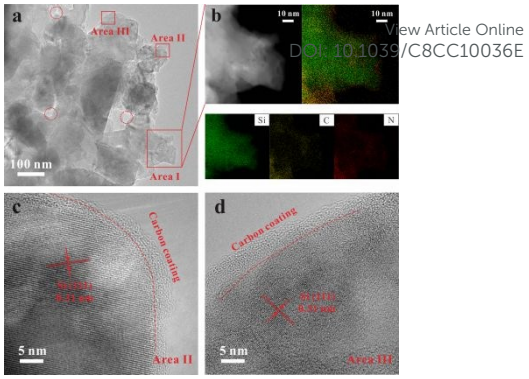

Fig. 3 The morphology and composition of Si/NG. (a) TEM image, (b) dark-field TEM image and EDS mapping of area I, and HRTEM images of area II (c) and area III (d).

and subsequent low-temperature chemical reduction. The organoclay precursors, prepared by simply intercalating montmorillonite (Mt) with crystal violet (CV, Fig. S1), was simultaneously served as the sources of silicon, carbon, and nitrogen. The resulting Si/NG exhibited hierarchical porous architecture, large specific surface area (153 m^2 g^{-1}), and a lamellar morphology (Si flake coated by N-doped graphene-like carbon (NG)). As anode in LIBs, Si/NG showed an enhanced cycling performance (reversible capacity of 1138 mAh g^{-1} at 1.0 A g^{-1} after 240 cycles) and a good rate capability (~434 mAh g^{-1} at 8.0 A g^{-1}).

The schematic illustration displays the preparation process of S/NG (Fig. 1). Mt is a representative 2:1 type clay mineral composed of two tetrahedral (T) sheets sandwiching one octahedral (O) sheet.[18, 19] The inorganic cations within the interlayer space balance the negative charges (derived from isomorphous substitution) on the layers. The Mt/CV composite as precursor in this work was easily obtained through a cation exchange reaction between Mt and CV. Then, the thermal treatment under a N_2 atmosphere *in situ* converted CV to NG within the confined interlayer space of Mt. In return, the generated NG again acted as nanotemplates, inducing the newly formed Si nanocrystals to grow into Si flakes during subsequent aluminothermic reduction reaction. A high-purity Si/NG was finally obtained after selective acid washing. Our developed route for producing nanostructured Si/N-doped graphene composite has several distinct advantages: 1) this strategy is promising in scalable production owing to the facile procedure and low-cost precursor; 2) nanostructured Si is distributed uniformly in carbon matrix due to the *in-situ* synthesis; 3) the heteroatom doping is achieved along with the formation of NG within the confined interlayer space of Mt.

The X-ray diffraction (XRD) patterns of the samples at different stages during the synthesis of Si/NG were listed (Fig. 2a and b). The d_{001}-value of 1.51 nm for Mt showed a typical Ca^{2+} form with two H_2O layers between Mt layers.[20] The cation exchange reaction with CV caused a slight decrease in the basal spacing (1.48 nm), implying the replacement of hydrated Ca^{2+} by hydrophobic organic molecule within the interlayer space. After carbonization, Mt/CV was converted to the montmorillonite/carbon composite (Mt/C) with a basal spacing of 1.31 nm (Fig. S2). By subtracting the essential thickness of Mt layer (0.96 nm), the interlayer spacing of Mt/C is 0.35 nm, close to the thickness of carbon monolayer (i.e., graphene). This result implied the formation of a graphene-like carbon sheet within the confined interlayer space of Mt, which was further confirmed by the TEM image of the carbon material after the removal of Mt layers (Fig. S3). According the corresponding energy dispersive X-ray spectroscopy (EDS), the content of N atoms in NG was about 5.5 at.%. After the aluminothermic reaction (using Mt/C as precursor), the intermediate was collected, whose XRD pattern showed the characteristic reflections of Si and AlOCl, besides those of the starting materials Al and $AlCl_3$ (Fig. 2b). The phenomenon suggested the successful reduction of Mt to crystalline Si, probably *via* the reaction of $3SiO_2$ (s) + 4Al (s) + $2AlCl_3$ (l) → 3Si (s) + 6AlOCl (s).[21] The byproducts were removed by selective acid washing and then Si/NG was achieved. The XRD pattern of Si/NG exhibited the sharp reflections of crystalline Si,[22] consistent with those of bare Si obtained using Mt as precursor in the same conditions.

Scanning electron microscopy (SEM) images showed Si/NG displayed a morphology of flakes in uneven size (Fig. 2f and Fig. S4), similar to that of the precursor Mt/C (Fig. 2d); while bare Si presented irregular agglomerated particles (as marked in the red circles in Fig. 2e), although its precursor Mt also had a layered structure. The spherical particles/shells were also obtained with increasing the amount of reductant (Fig. S5a), consistent with the previous study.[23] The difference was attributed to the roles of NG within the interlayer space of Mt. During the aluminothermic reduction process, NG not only acted as an isolation barrier to keep Si nanocrystals from agglomerating, but also a nanotemplate to induce the newly formed Si nanocrystals to grow into Si flakes. However, without the presence of NG, the Si nanocrystals tended to aggregate and eventually grow into spherical or irregular large particles (Fig. 2e and Fig. S5).

Transmission electron microscopy (TEM) images of Si/NG disclosed that the irregular flakes cross-linked and/or overlapped (Fig. 3a and Fig. S4), forming hierarchical pores (i.e., mesopores and macropores) (as marked in the red circles in Fig. 3a). The interplanar spacing of 0.31 nm assigned to (111) plane of crystalline Si appeared in the high-resolution TEM of Si/NG, suggesting the formation of well-crystallized Si. Interestingly,

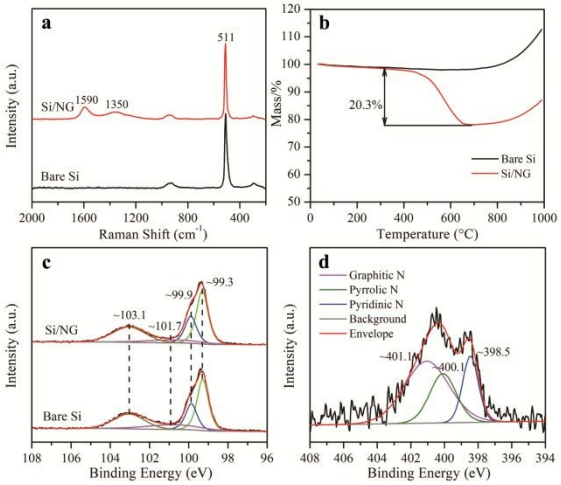

Fig. 4 Characterization of Si/NG and bare Si. (a) Raman spectra, (b) TG curves in air, and (c) high resolution Si2p XPS spectra. (d) High resolution N1s XPS spectrum of Si/NG.

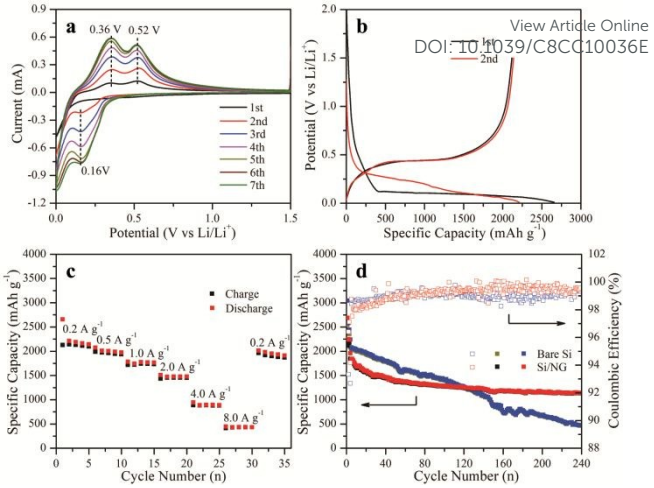

Fig. 5 Electrochemical performance of the Si/NG electrodes. (a) Cyclic voltammetry curves at a scan rate of 0.1 mV s^{-1} in the voltage range of 0.001–1.5 V (*vs*. Li/Li^+); (b) discharge-charge curves at a current density of 0.2 A g^{-1} between 0.001 and 1.5 V (*vs*. Li/Li^+); (c) rate capability at various current densities from 0.2 to 8.0 A g^{-1}; (d) comparative cycling performance of the Si/NG and bare Si electrodes at current densities of 0.2 A g^{-1} for the initial three cycles and 1.0 A g^{-1} for the remaining cycles.

we observed that an approximately 4-nm-thick and less than 1-nm-thick carbon layer tightly wrapped around the Si nanocrystals (Fig. 3c and Fig. S4c). Similar phenomenon was visible in Fig. 3d, but the lattice fringes of Si became faint, which could be attributed to the effect of carbon coating on the surface of crystalline Si. In addition, the dark-field TEM image and EDS mapping demonstrated that Si, C, and N were uniformly distributed on Si/NG, and the coating structure could be clearly observed (Fig. 3b). Based on the results in our work and previous studies[23-26], we also provided a probable reaction mechanism from Mt/C to Si/NG (Fig. S6).

The Raman spectra of both Si/NG and bare Si showed intense Raman bands at ~511 cm^{-1} (Fig. 4a), arising from the first-order optical phonon mode of Si.[27] These Raman bands red-shifted and the full width at half maximum broadened, compared with the monocrystalline Si (~521 cm^{-1}), which were attributed to the decrease in sizes.[27, 28] Moreover, two clear Raman bands at 1350 and 1590 cm^{-1} were observed for Si/NG, corresponding to D-band (from the disordered carbon atoms) and G-band (from sp^2-hybridized structure), respectively.[16, 29] The I_D/I_G value (~1.5) suggested the partially graphitic nature. The content of carbon in Si/NG was measured *via* thermogravimetry (TG) analysis in air (Fig. 4b). TG curve of bare Si indicated no obvious mass change before 700°C, and then a slow rise of weight because of the oxidation of Si; while that of Si/NG showed a significant mass loss from 300 to 700°C, due to the oxidation and decomposition of amorphous carbon, implying ~20.3 wt.% NG in the composite.

The high resolution Si2p X-ray photoelectron spectroscopy (XPS) spectra of Si/NG and bare Si exhibited the similar characteristics and were fitted into four components at 99.3, 99.9, 101.7, and 103.1 eV (Fig. 4c). The first two primary peaks corresponded to Si $2p_{3/2}$ and Si $2p_{1/2}$ of elemental Si, while the latter two could be assigned to SiO_x derivatives with various oxidation states,[28] derived from the post-oxidation of crystalline Si and/or the incomplete reduction of Si-O tetrahedral (Fig. S7). Noticeably, besides Si, C, and O, N was also detected in XPS survey spectrum of Si/NG (Fig. S8), which was derived from CV.

The absence of other metal elements manifested a high-purity of Si/NG. The high resolution N1s spectrum was deconvolved into three peaks at 398.5, 400.1, and 401.1 eV (Fig. 4d), assigned to pyridinic, pyrrolic, and graphitic N, respectively.[17, 30] The XPS results further confirmed that Si/NG was composed of Si and N-doped carbon. In addition, Si/NG had a larger specific surface area (153 m^2 g^{-1}) and total pore volume (0.26 cm^3 g^{-1}) than bare Si (131 m^2 g^{-1} and 0.18 cm^3 g^{-1}), calculated according to N_2 adsorption/desorption isotherms (Fig. S9).

The electrochemical properties of Si/NG as an anode were assessed in a CR2032 coin-type half-cell. As shown by the cyclic voltammetry curves (Fig. 5a), a very weak and broad peak at 0.5~0.8 V occurred but disappeared from the second scan onwards, implying the generation of irreversible solid electrolyte interphase (SEI) films[31] (directly verified by the SEM images and XPS spectrum of Si/NG after cycling (Fig. S10)). Meanwhile, a sharp cathodic peak (at < 0.1 V) and two anodic peaks (at 0.36 and 0.52 V) were observed, corresponding to the lithiation process of Si and two-step delithiation reaction from Li_xSi to amorphous Si, respectively.[23] In subsequent cycles, a new reductive peak at 0.16 V gradually emerged, due to the transformation of crystalline Si to amorphous phase in the first cycle,[10, 32] which was further confirmed by XRD patterns of the Si/NG electrodes after different cycles (Fig. S11). Both reductive and oxidative peaks enhanced in intensity in the first few cycles and then overlapped, suggesting a kinetic enhancement process before stabilization for the Si/NG electrode.[31-33] The lithiation/delithiation processes of Si/NG were similar to those of raw Si anodes in previous reports,[23, 28] suggesting that Si was the main component in the composite. Moreover, all of the voltage platforms in the galvanostatic charge/discharge profiles (Fig. 5b) matched well with the above reductive/oxidative peaks. The Si/NG electrode delivered an initial specific discharge/charge capacity of 2657/2127 mAh g^{-1} with a high initial Coulombic efficiency (CE) of 80%. The capacity loss was

generally related to the inevitable formation of SEI films and side reactions between electrolytes and active materials.[31]

The Si/NG electrode showed the reversible capacities of ~2187, 2002, 1773, 1475, 892, and 434 mAh g^{-1} at current densities of 0.2, 0.5, 1.0, 2.0, 4.0, and 8.0 A g^{-1} (Fig. 5c), respectively. When the current density went back to 0.1 A g^{-1}, the specific capacity was almost recovered, manifesting an outstanding rate capability. The cycling performance of the Si/NG electrode at a large current density was further investigated (Fig. 5d). A high reversible capacity of 1138 mAh g^{-1} at 1.0 A g^{-1} was still maintained after 240 cycles, suggesting a good cycling stability of the Si/NG electrode. By contrast, the bare Si electrode underwent a serious capacity fading upon cycling (Fig. 5d and Fig. S12), although its specific capacity at the beginning was higher than that of Si/NG due to the much higher theoretical specific capacity of Si than that of graphene.[5] Moreover, the Si/NG electrode displayed a lower CEs than bare Si at first, associated with the larger specific surface area of Si/NG (facilitating the production of SEI films). The CEs of Si/NG increased upon cycling and surpassed those of bare Si after ~50 cycles, and reached over 99%. Besides, the Nyquist plots revealed that the Si/NG electrode had lower charge-transfer impedance and diffusion impedance to lithium ions than bare Si electrode, as confirmed by the smaller semicircle in the high-frequency region and the large slope in the low-frequency range (Fig. S13).[9, 33] The TEM images of electrodes after cycling showed that Si/NG remained intact and kept the original morphology in comparison with bare Si (Fig. S14 and S15). The outstanding cyclic performance of Si/NG could be attributed to the enhanced structural/interfacial stability and electronic conductivity resulting from the N-doped carbon coating, in which N-doping further improved the electronic conductivity and active sites toward lithium.[16] Compared to other Si/C composite anodes, Si/NG exhibited excellent electrochemical properties from a practical point of view (Table S1).

In summary, silicon flake/N-doped graphene-like carbon composite was synthesized from organoclay *via* an *in-situ* strategy. Clay sheets first acted as nanotemplates during the formation of N-doped graphene-like carbon; in return, the generated carbon sheets acted as nanotemplates for *in situ* synthesizing silicon flakes during aluminothermic reaction. As anode material in LIBs, Si/NG exhibited an enhanced cycling performance and a good rate capability. This work offered a facile and low-cost method for synthesizing silicon/heteroatom-doped graphene composite from organoclay, which would be very potential in the practical production and commercial application of advanced anode materials in LIBs.

This work was financially supported by National Natural Science Foundation of China (41572031), National Program for Support of Top-notch Young Professionals, Guangdong Special Support Program, and Science and Technology Planning Project of Guangdong Province, China (2017B030314175).

Conflicts of interest

There are no conflicts to declare.

Notes and references

1 S. Chu and A. Majumdar, *Nature*, 2012, **488**, 294.
2 N. Nitta, F. Wu, J. T. Lee and G. Yushin, *Mater. Today*, 2015, **18**, 252-264.
3 J. K. Lee, C. Oh, N. Kim, J.-Y. Hwang and Y.-K. Sun, *J. Mater. Chem. A*, 2016, **4**, 5366-5384.
4 Y. Sun, N. Liu and Y. Cui, *Nature Energy*, 2016, **1**, 16071.
5 K. Feng, M. Li, W. Liu, A. G. Kashkooli, X. Xiao, M. Cai and Z. Chen, *Small*, 2018, **14**, 1702737.
6 M. Sohn, H.-I. Park and H. Kim, *Chem. Commun.*, 2017, **53**, 11897-11900.
7 W. Li, X. Sun and Y. Yu, *Small Methods*, 2017, **1**, 1600037.
8 M. A. Rahman, G. Song, A. I. Bhatt, Y. C. Wong and C. Wen, *Adv. Funct. Mater.*, 2016, **26**, 647-678.
9 Y. Chen, Y. Lin, N. Du, Y. Zhang, H. Zhang and D. Yang, *Chem. Commun.*, 2017, **53**, 6101-6104.
10 Q. Yun, X. Qin, W. Lv, Y.-B. He, B. Li, F. Kang and Q.-H. Yang, *Carbon*, 2015, **93**, 59-67.
11 S. Chen, L. Shen, P. A. van Aken, J. Maier and Y. Yu, *Adv. Mater.*, 2017, **29**, 1605650.
12 J.Y. Luo, X. Zhao, J.S. Wu, H. D. Jang, H. H. Kung and J.X. Huang, *J. Phys. Chem. Lett.*, 2012, **3**, 1824-1829.
13 S. Han, D. Wu, S. Li, F. Zhang and X. Feng, *Small*, 2013, **9**, 1173-1187.
14 L. Zhang, X. Liu, Q. Zhao, S. Dou, H. Liu, Y. Huang and X. Hu, *Energy Storage Mater.*, 2016, **4**, 92-102.
15 P. Avouris and C. Dimitrakopoulos, *Mater. Today*, 2012, **15**, 86-97.
16 A. L. M. Reddy, A. Srivastava, S. R. Gowda, H. Gullapalli, M. Dubey and P. M. Ajayan, *ACS Nano*, 2010, **4**, 6337-6342.
17 J. Lin, J. He, Y. Chen, Q. Li, B. Yu, C. Xu and W. Zhang, *Electrochim. Acta*, 2016, **215**, 667-673.
18 R. L. Zhu, Q. Z. Chen, Q. Zhou, Y. F. Xi, J. X. Zhu and H. P. He, *Appl. Clay Sci.*, 2016, **123**, 239-258.
19 F. Bergaya and G. Lagaly, in *Developments in Clay Science*, ed. F. Bergaya and G. Lagaly, Elsevier, 2013, vol. 5, pp. 1-19.
20 Q. Z. Chen, R. L. Zhu, L. Y. Ma, Q. Zhou, J. X. Zhu and H. P. He, *Appl. Clay Sci.*, 2017, **135**, 129-135.
21 N. Lin, Y. Han, J. Zhou, K.L. Zhang, T.J. Xu, Y.C. Zhu and Y.T. Qian, *Energy Environ. Sci.*, 2015, **8**, 3187-3191.
22 X. Zhou, Y. Ren, J. Yang, J. Ding, J. Zhang, T. Hu and J. Tang, *Chem. Commun.*, 2018, **54**, 12214-12217.
23 Z.-W. Zhou, Y.-T. Liu, X.-M. Xie and X.-Y. Ye, *Chem. Commun.*, 2016, **52**, 8401-8404.
24 K. Mishra, J. Zheng, R. Patel, L. Estevez, H. Jia, L. Luo, P. Z. El-Khoury, X. Li, X.-D. Zhou and J.-G. Zhang, *Electrochim. Acta,* 2018, **269**, 509-516.
25 P. Gao, X. Huang, Y. Zhao, X. Hu, D. Cen, G. Gao, Z. Bao, Y. Mei, Z. Di and G. Wu, *ACS Nano*, 2018, **12**, 11481-11490.
26 G. Song, J. Ryu, J. C. Kim, J. H. Lee, S. Kim, C. Wang, S. K. Kwak and S. Park, *Commun. Chem.*, 2018, **1**, 42.
27 R. P. Wang, G. W. Zhou, Y. L. Liu, S. H. Pan, H. Z. Zhang, D. P. Yu and Z. Zhang, *Phys. Rev. B*, 2000, **61**, 16827-16832.
28 Q.Z. Chen, R.L. Zhu, S.H Liu, D.C. Wu, H.Y. Fu, J.X. Zhu and H.P. He, *J. Mater. Chem. A*, 2018, **6**, 6356-6362.
29 J. Feng, Z. Zhang, L. Ci, W. Zhai, Q. Ai and S. Xiong, *J. Power Sources*, 2015, **287**, 177-183.
30 S.H. Liu, Y.F. Dong, C.T. Zhao, Z.B. Zhao, C. Yu, Z.Y. Wang and J.S. Qiu, *Nano Energy*, 2015, **12**, 578-587.
31 J. Zhu, J. Yang, Z. Xu, J. Wang, Y. Nuli, X. Zhuang and X. Feng, *Nanoscale*, 2017, **9**, 8871-8878.
32 Y. Zhou, H. Guo, G. Yan, Z. Wang, X. Li, Z. Yang, A. Zheng and J. Wang, *Chem. Commun.*, 2018, **54**, 3755-3758.
33 F. Wu, H. Wang, J. Shi, Z. Yan, S. Song, B. Peng, X. Zhang and Y. Xiang, *ACS Appl. Mater. Inter.*, 2018, **10**, 19639-19648.